Dislocation Mobility in Copper*

W. Frank Greenman, Thad Vreeland, Jr., and David S. Wood
W. M. Keck Laboratories, California Institute of Technology, Pasadena, California
(Received 8 March 1967)

The velocity of dislocations of mixed edge–screw type in copper crystals of 99.999% purity has been measured as a function of stress at room temperature. Dislocation displacements produced by torsion stress pulses of microsecond duration were detected by etch pitting {100} surfaces. A nearly linear relationship between dislocation velocity and resolved shear stress was found. Stresses from 2.8×10^6 to 23.1×10^6 dyn/cm^2 produced velocities from 160 to 710 cm/sec. These data give a value of the damping constant for high-velocity dislocations of 7×10^{-4} dyn·sec/cm^2, in good agreement with the values deduced from internal-friction measurements. The results also agree, within experimental and theoretical uncertainties, with the phonon viscosity model for the mobility of dislocations.

INTRODUCTION

The velocities of dislocations have been determined from direct observations of the dislocation displacements produced by known stresses applied for known periods of time in lithium fluoride,[1] silicon–iron,[2,3] sodium chloride,[4] tungsten,[5] and various semiconductor crystals.[6,7] The purpose of this paper is to present the results of the first such direct determination of dislocation velocity in a fcc metal, copper. The experiments were all performed at room temperature.

TEST SPECIMENS

Experiments were performed on single-crystal copper specimens in the form of right circular cylinders 1.25 cm in diameter and from 1.48 to 1.90 cm long. The cylindrical surface was modified by four flat {100} observation surfaces, each about 0.3 cm wide, spaced at 90° intervals around the circumference and extending the full length of the specimen. The cylindrical axis was parallel to the [100] crystal axis to within $\pm\frac{1}{2}°$.

These test specimens were machined from single crystals about 2.5 cm in diameter and 12.5 cm long. The crystals were grown in graphite crucibles from a charge of 99.999% copper by the modified Bridgman technique employed by Young and Savage.[8] Some of the crystals were grown in the authors' laboratory in a vacuum of 5×10^{-4} Torr or less. Others, which were kindly supplied by the Sandia Corporation, Albuquerque, New Mexico, were grown in a helium atmosphere. Rough machining of specimens was performed by trepanning and wire-slicing using spark-erosion machines. Finish machining was accomplished by chemical lapping using a saturated solution of cupric chloride in concentrated hydrochloric acid and a rotating cloth-covered Lucite wheel. At least 0.04-cm thickness of material was removed by chemical lapping, thus removing the mechanical surface damage due to spark-erosion machining. The test specimens were annealed for about 100 h at 1030°±10°C in a hydrogen atmosphere after finish machining.

EXPERIMENTAL TECHNIQUES

Single torsional stress pulses of microsecond duration were applied to the specimens by means of the machine described by Pope *et al.*[9] This machine utilizes zero-order-mode torsional waves in cylindrical bars which are generated in the following manner. An initial static torque is applied to a section of a cylindrical rod which is a part of the torsion rod or load train shown schematically in Fig. 1. The torque is applied to the top of the section by dead weight loading of a cranking disk attached to the rod through a rubber sleeve. A 0.015-cm-thick glass disk cemented to the bottom of the section transmits this torque to a Bakelite fixture which is attached to a fixed bearing tube surrounding the rod. A 0.005-cm-thick aluminum foil is cemented between the glass disk and Bakelite with Eastman 910 adhesive. The lower section of the torsion rod or load train is attached to the opposite side of the glass disk by means of a butt adhesive bond. This section of the torsion rod is coaxial with the upper section but does not carry any static torque. The specimen is attached to the bottom end of this lower section of the torsion rod, and the bottom end of the specimen is the free end of the torsion rod system. The section of the rod above the cranking disk is coated with a viscoelastic material in order to attenuate the waves propagating away from the specimen.

The application of the stress pulse to the specimen is initiated by a high-voltage capacitor discharge through the aluminum foil. Explosion of the foil releases the static torque and results in elastic waves which propagate away from the glass disk interface of

* This work was supported by the U. S. Atomic Energy Commission.

[1] W. G. Johnston and J. J. Gilman, J. Appl. Phys **30**, 129 (1959).
[2] D. F. Stein and J. R. Low, Jr., J. Appl. Phys. **31**, 362 (1960).
[3] J. S. Erickson, J. Appl. Phys. **33**, 2499 (1962).
[4] E. Yu. Gutmanas, E. M. Nadgornyi, and A. V. Stepanov, Soviet Phys.—Solid State **5**, 743 (1963).
[5] H. W. Schadler, Acta Met. **12**, 861 (1964).
[6] A. R. Chaudhuri, J. R. Patel, and L. G. Rubin, J. Appl. Phys. **33**, 2736 (1962).
[7] M. N. Kabler, Phys. Rev. **131**, 54 (1963).
[8] F. W. Young, Jr., and J. R. Savage, J. Appl. Phys. **35**, 1917 (1964).
[9] D. P. Pope, T. Vreeland, Jr., and D. S. Wood, Rev. Sci. Instr. **35**, 1351 (1964).

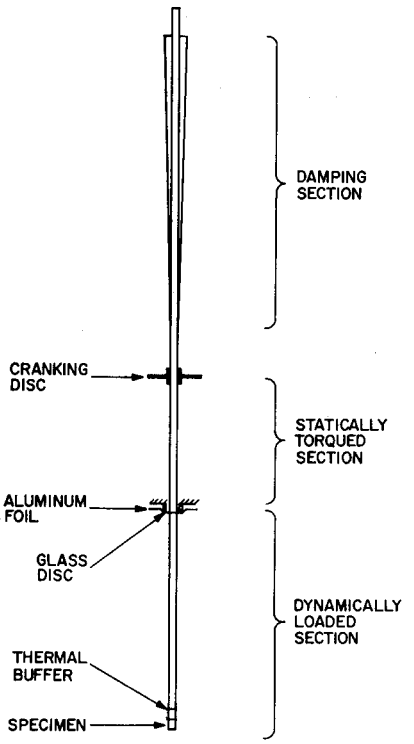

FIG. 1. Schematic diagram of torsion-pulse machine.

the torsion rod. The amplitude of the dynamic torque in the lower section of the torsion rod is one-half the initial static torque applied to the machine and, therefore, proportional to the weight hung on the cranking disk. The duration of the stress pulse at any point in the speciman is the time required for the wave to propagate from that point to the free end and return.

The stress wave generated by the release of the static torque propagates without dispersion through the isotropic elastic rod attached to the glass disk because the elastic zero-order-mode torsional waves are nondispersive. The propagation of zero-order-mode torsional waves in the ⟨100⟩-oriented copper single-crystal specimen is also nondispersive and the distribution of shear stress over a cross section of the specimen is the same as that in an isotropic material.

The materials and dimensions of the rod system of the torsion machine were chosen so as to make the acoustic impedance of all the rod sections equal to that of the specimen. Torsional-wave reflections at the interfaces between different materials in the load train were thereby avoided. The rods were made of steel 1.27 cm in diameter. This provided an acoustic match with specimens of 1.25 cm diameter. A thermal buffer rod of polycrystalline copper, 2.3 cm long and 1.33 cm in diameter, was cemented between the steel torsion rod and the copper specimen. This prevented spurious stresses in the specimens due to differential thermal expansion of the steel and copper while maintaining the acoustic impedance match. A conical joint of 30° included angle was made in the lower steel rod at a point 7.6 cm above the thermal buffer. This facilitated removal of the specimen for polishing and etching. These several portions of the specimen–torsion-rod system were joined together by means of Eastman 910 adhesive. The conical joint in the steel rod was parted by the rapid application of heat from a gas torch when it was desired to remove the specimen from the machine in order to etch and observe the dislocations. A photograph of a test specimen cemented onto the thermal buffer and end section of the steel torsion rod is shown in Fig. 2.

The amplitude and duration of the stress pulse were measured by means of silicon strain gauges, cemented to the steel torsion rod at a point 18.1 cm from the thermal buffer. The strain-gauge output voltage was displayed on both beams of a Tektronic type 555 oscilloscope. The upper beam was triggered by the capacitor discharge employed to initiate the torsion wave and had a sweep rate of 200 μsec/cm. This provided information about any reflected stress pulses applied to the specimen at relatively long times after the primary stress pulse. The initiation of the lower trace was delayed about 116 μsec, and the sweep rate was 20 μsec/cm. This provided detailed information regarding the primary stress pulse.

Fresh dislocations were introduced into specimens by scratching the {100} observation surfaces in a controlled manner with a diamond phonograph stylus or an alumina whisker by means of a special scratching apparatus. Scratching was performed after the surface had been chemically polished in the manner employed by Livingston.[10]

Two etches were used to reveal dislocations on the {100} observation surfaces of the specimens. Etching for 3 sec in the solution used by Livingston[10] produced about the same pit size as etching for 5 sec in the solution used by Young.[11] Immersion in either etchant was followed by a rinse in hydrobromic acid.

Specimens were etched prior to stress application to reveal the grown in dislocations and the fresh dis-

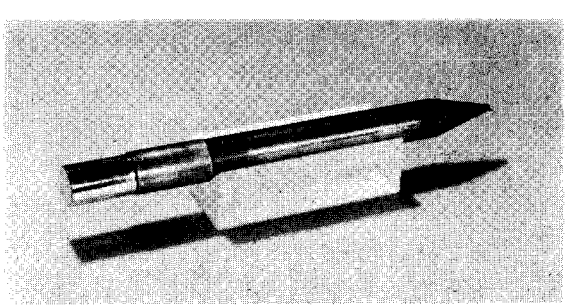

FIG. 2. Test specimen, thermal buffer, and torsion-rod end-section assembly.

[10] J. D. Livingston, J. Australian Inst. Metals **8**, 15 (1963).
[11] F. W. Young, Jr., J. Appl. Phys. **32**, 192 (1961).

locations produced by scratching. A permanent record of this dislocation configuration was obtained by making a replica of the specimen surface on a cellulose acetate film.

Immediately after testing, the specimen was rinsed in distilled water, chemically polished for about 10 sec, etched, and rinsed in hydrobromic acid and distilled water. The 10-sec chemical polish did not remove the prior dislocation etch pits. It prepared the {100} surfaces so that the subsequent application of etchant was less likely to produce general faceting which obscured the dislocation etch pits. After this second etching, the observation surfaces were replicated again. When general faceting did occur during the second etching, the specimen was chemically polished long enough to remove the prior etch pattern and then re-etched and replicated. This latter procedure precluded use of the double-etch technique of discerning dislocation displacement on the second replica alone. Dislocation displacement could be determined nevertheless by comparing the first and second replicas.

The blink microscope system developed by Pope *et al.*[12] was employed to compare the first and second replicas in order to determine dislocation displacements. This system superimposes the images formed by two microscope objective lenses in one field of view and displays the two images alternately in time at a frequency of about 1 cps. The new positions to which individual dislocations had moved during the stress pulse could then be determined by "blinking."

Considerable care was required to determine the original position of a given dislocation which had moved. It was assumed that the original position of a dislocation must have been somewhere along one of the two traces of {111} slip planes which pass through the final position of that dislocation. Use of the "double-etch" technique, where possible, was also helpful in determining the original position of a displaced dislocation because the original etch pit is flat bottomed, since the dislocation was not there during the second etch. Use of a scratched specimen was also helpful because nearly all original dislocation positions are very near the scratch.

The distances between the original and final positions of individual dislocations were measured to within ± 4 μ using a filar micrometer eyepiece in the microscope. Dislocation displacements were measured at a minimum of three different stations along the axial length of each specimen. On the average, the displacements of 24 different dislocations were measured at each station along each specimen tested.

Four tests were performed with nominal resolved shear stresses at the outer radius of the specimen ranging from 2.5×10^6 to 25×10^6 dyn/cm^2. A different speciman was used in each test.

[12] D. P. Pope, T. Vreeland, Jr., and D. S. Wood, Rev. Sci. Instr. **37**, 377 (1966).

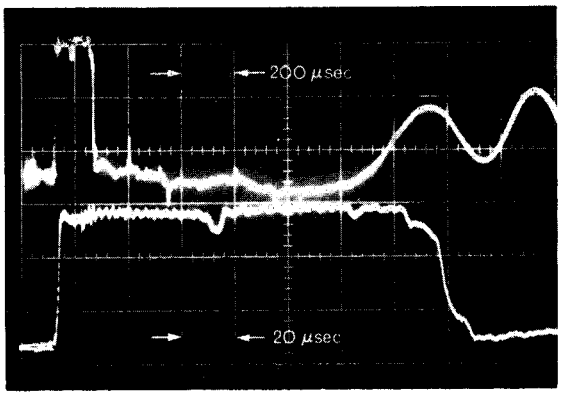

FIG. 3. Torsion-bar strain-gauge signal vs time for specimen number 6-2-1.

RESULTS

The photographic record of the oscilloscope traces of the torsion bar strain-gauge signal which was obtained during the test of specimen number 6-2-1 is shown in Fig. 3. The upper trace, at a sweep rate of 200 μsec/cm, shows that some waves reflected from the damping section of the testing machine reach the strain gauges about 1100 μsec after the primary wavefront. These late arriving waves produce a stress in the test specimen of only about 3% of the stress produced by the primary wave because they rise in a time which is much longer (about 300 μsec) than the time for an elastic wave to make a round trip transit of the test specimen (10.0 μsec). Thus, the only significant stress acting on the test specimen is due to the primary incident torsion wave and the associated waves reflected from the specimen.

The lower oscilloscope trace in Fig. 3, at a sweep rate of 20 μsec/cm, shows the details of the primary incident wave and the wave reflected from the test specimen. The rise time of the incident wave is seen to be about 2 μsec. About 60 μsec after the arrival of the incident wave, a small dip in the trace may be seen. This is a small disturbance caused by the conical joint in the steel torsion rod. A second small dip in the record occurs about 115 μsec after the initial wavefront. This is a small disturbance produced at the interface between the steel torsion rod and the thermal buffer.

The wave which is reflected from the specimen begins 135 μsec after the initial rise in the lower trace in Fig. 3. At this point there is a small drop in torque which does not recover. This shows that the maximum torque transmitted into the specimen was a little less than the torque amplitude of the incident wave. Therefore, it must be concluded that a small plastic wave as well as an elastic wave was initiated in the specimen by the incident wave. At 146 μsec after the initial rise on the record, a large and rapid drop in torque occurs. This is the result of the elastic portion of the wave which is transmitted through the specimen to the free end and returns as an elastic unloading wave. The fact

TABLE I. Experimental results.

Specimen number	Diameter D (cm)	Length l (cm)	Max. torque T_m (10^6 dyn·cm)	Stress pulse times (μsec) t_1	t_2	t_3	Loaded-end dislocation displacement d (μ)
6-3-1	1.25	1.90	2.65	3	15	27	31.5
3-2-1	1.25	1.50	6.34	2	10	23	40
3-3-1	1.25	1.48	12.3	3	14	18	55.9
6-2-1	1.25	1.54	21.8	2	12	21	110.3

that this unloading wave does not reduce the torque completely to zero also shows that a portion of the wave in the specimen was a wave of plastic deformation. The final small portion of the unloading phase of the pulse shown in Fig. 3 represents that portion of the wave in the specimen which propagated from the thermal buffer interface to the free end as a plastic wave and returned from the free end as an elastic unloading wave.

These results show that the major portion of the torsional wave in the specimen propagated in an elastic manner. Thus, to a first approximation, the magnitude of the stress is independent of position along the specimen and the duration of stress is linearly proportioned to distance from the free end of the specimen.

The maximum torque transmitted into each test specimen was determined from the portion of the strain gauge record which began 135 μsec after the initial rise in the record as discussed above. The relationship between torque and the strain-gauge signal voltage is readily obtained from the fact that the signal voltage during the relatively long period of essentially constant trace deflection prior to the arrival of reflected waves at the strain gauges corresponds to one-half the initial static torque applied in the torsion machine. Values of the maximum torque transmitted to the specimen, T_m, obtained in this way for the four tests are given in the fourth column of Table I. The maximum shear stress, $\bar{\tau}_m$, acting at the periphery of cross sections normal to the specimen axis is obtained from the torque by the usual formula for torsion of cylindrical rods, namely

$$\tau_m = 16T_m/\pi D^3, \tag{1}$$

where D is the diameter of the specimen, as listed in the second column of Table I. The maximum resolved shear stress, τ_m, acting on {111} ⟨110⟩ slip systems can be shown to be

$$\tau_m = (1/6^{1/2})\bar{\tau}_m. \tag{2}$$

Thus by combining Eqs. (1) and (2), the maximum resolved shear stress is related to the maximum torque transmitted into the specimen by

$$\tau_m = (16/\pi 6^{1/2})(T_m/D^3). \tag{3}$$

Values of maximum resolved shear stress for each test performed are given in the second column of Table II.

There are three ⟨110⟩ slip directions on each {111} slip plane. One of these slip directions lies in the {100} observation surface. The resolved shear stress acting on this particular slip system is zero, however. The other two ⟨110⟩ slip directions are inclined to the observation surface and the resolved shear stress acting on these later two slip systems is the value given by Eq. (3).

The dislocation lines extending into the interior of the test specimen from the observed etch pits are probably oriented nearly at right angles to the ⟨110⟩ trace of the {111} slip planes on the {100} observation surface. The slip directions which are subjected to a nonzero resolved shear stress are inclined to this direction of the dislocation lines. Thus the dislocations which were observed to move in these tests were probably of mixed edge–screw type.

The torque vs time relation in the test specimen is known exactly only at the end of the specimen which is cemented to the thermal buffer rod (this is designated as the "loaded end" hereafter). The reason for this is the presence of a significant amount of plastic wave propagation in the specimen. The torque-vs-time relation at the loaded end of the specimen may be determined unambiguously from the test records because both the incident and reflected waves which propagate between the strain gauges and the loaded end of the specimen are purely elastic and propagate at known wave velocities. The torque-vs-time relation at the loaded end of specimen number 6–2–1 is shown by the

TABLE II. Calculated results.

Specimen number	Max. resolved shear stress τ_m (10^6 dyn/cm^2)	Uncorrected dislocation velocity v (cm/sec)	Corrected dislocation velocity v' (cm/sec) $m=0.7$	$m=1.0$
6-3-1	2.82	240	150	160
3-2-1	6.74	390	240	260
3-3-1	13.1	550	370	390
6-2-1	23.2	1040	670	710

solid line in Fig. 4. The experimentally determined relation was approximated by the trapezoidal-shaped relation shown by the dashed line, for the purpose of determining dislocation velocities in the manner to be explained. Similar torque-vs-time relations were determined for all tests. The times t_1, t_2, and t_3 from the beginning of these trapezoidal stress pulses to the beginning and end of the maximum stress period and the end of the pulse, respectively, are listed for each of the four tests in the fifth, sixth, and seventh columns of Table I.

Photomicrographs of the replicas of specimen number 3-3-1 taken before (a) and after (b) the application of the stress pulse are shown in Fig. 5. The scratch (horizontal in the photomicrographs) is parallel to the longitudinal axis of the specimen. The same area of the specimen is identified by the segment of the substructure boundary in the lower right-hand corner of these two photomicrographs. Two examples of dislocation displacement are indicated at A and B in Fig. 5(b).

The points representing mean values of measured dislocation displacement are plotted as a function of distance from the free end of the specimen in Fig. 6 for the four tests conducted. The number of individual dislocation displacements measured is indicated near each plotted point. The vertical lines through the plotted points represent the standard deviation of the measurements. The maximum standard deviation is 13% of the mean dislocation displacement. The straight lines in Fig. 6 were drawn to represent the data. This shows that the dislocation displacement is linearly proportional to distance from the free end of the specimen. The points marked "x" at the end of each line in Fig. 6 represent the extrapolated value of dislocation displacement d at the loaded end of each specimen. These values are given in the eighth column of Table I.

The observed linear relationship between dislocation displacement and distance from the free end of the specimen is consistent with the assumptions that the stress wave propagates through the specimen in an elastic manner and that the acceleration time for the dislocations is negligible. According to these approximations, the duration of stress Δt is related to distance

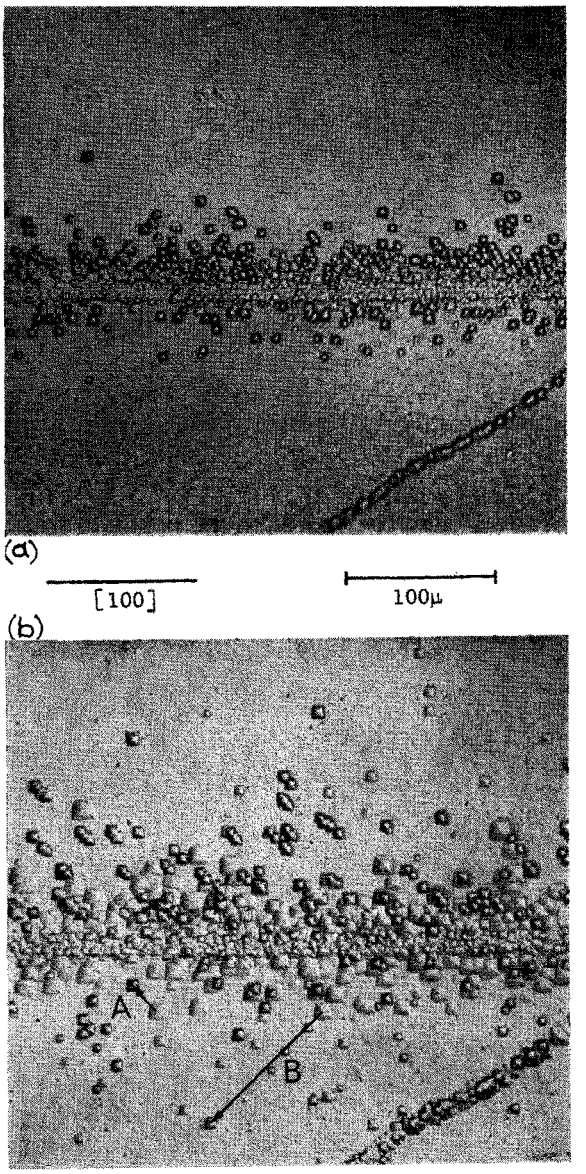

FIG. 5. Etch pits near scratch on specimen number 3-3-1. Before (a) and after (b) testing.

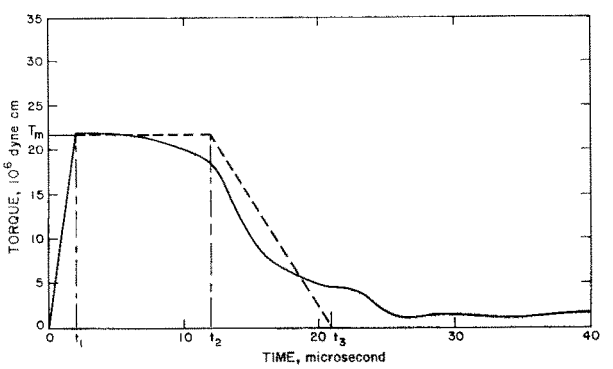

FIG 4. Torque vs time at loaded end of specimen number 6-2-1.

from the free end of the specimen x by

$$\Delta t = 2x/c, \tag{4}$$

where $c = 0.290 \times 10^6$ cm/sec is the velocity of propagation of an elastic torsional wave along the ⟨100⟩ specimen axis. Thus, if Eq. (4) is employed to convert the abscissa scale of Fig. 6 to a scale of time duration of stress, then the slopes of the lines are equal to the dislocation velocity. First approximation values of dislocation velocity v determined in this manner are given in the third column of Table II.

The first approximation values of dislocation velocity v are found to be approximately proportional to the $m = 0.7$ power of the maximum resolved shear τ_m when

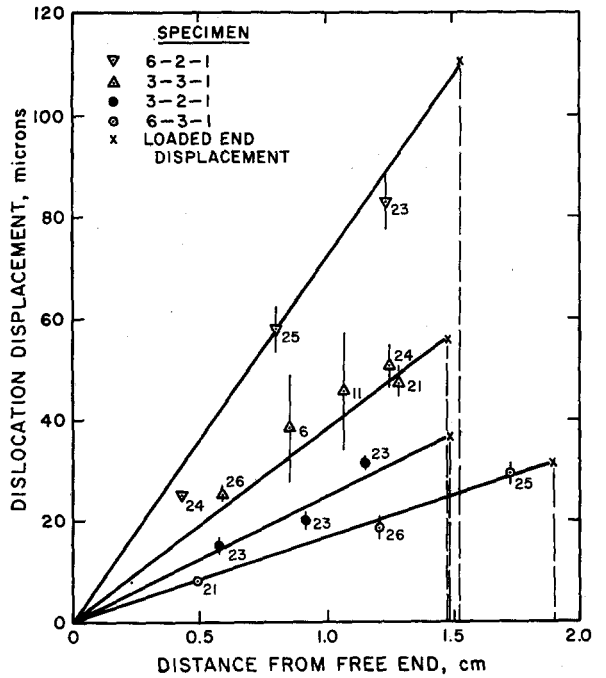

FIG. 6. Dislocation displacement vs distance from the free end of the specimen.

these data are fitted to an equation of the form

$$v=v_0(\tau_m/\tau_0)^m, \tag{5}$$

where m and τ_0 are material constants and v_0 is unit velocity. This result indicates, however, that a significant portion of the total dislocation displacement occurs during the rising and falling portions of the trapezoidal stress pulses such as that shown in Fig. 4. For this reason a more refined method of analysis of the experimental measurements has been employed to obtained corrected values of dislocation velocity v' as a function of resolved shear stress, τ_m.

The corrected dislocation velocity vs stress relation is obtained in the following manner: First, it is assumed that the relationship is of the form given by Eq. (5). Second, it is assumed that the torque-vs-time relations at the loaded ends of the specimens are the trapazoidal-shaped relations exemplified by Fig. 4 and defined by the values of T_m, t_1, t_2, and t_3 given for each test in Table I. Then it can be shown that the dislocation displacement at the loaded end of the specimen is given by

$$d'=v_0\left(\frac{\tau_m}{\tau_0}\right)^m\left[(t_2-t_1)+\frac{(t_1-t_2+t_3)}{(m+1)}\right], \tag{6}$$

where τ_m is the maximum stress during the stress pulse as given in Table II, and m and τ_0 are the undetermined material constants in Eq. (5).

Various values of material constants, m and τ_0, were chosen so as to minimize the quantity

$$e=\tfrac{1}{4}\sum_{n=1}^{4}\frac{d_n-d_n'}{d_n}, \tag{7}$$

where d_n and d_n' are the experimental and calculated values respectively of loaded-end displacement for the nth test. The "best fit" values of m and τ_0 determined in this manner are $m=0.7$ and $\tau_0=0.25\times10^4$ dyn/cm^2. The corresponding mean error is $e=0.088$. Thus, the "best fit" relation between the velocity of dislocations v in copper and the applied resolved shear stress τ is

$$v=v_0(\tau/0.25\times10^4)^{0.7}, \tag{8}$$

where τ is expressed in units of dynes per square centimeter.

A convenient graphical representation of the "fit" between the experimental data and Eq. (8) may be obtained as follows: The dislocation velocity v_m corresponding to the maximum resolved shear stress τ_m during the experimentally determined stress pulse is

$$v_m=v_0(\tau_m/\tau_0)^m. \tag{9}$$

Thus the theoretical dislocation displacement at the loaded end, Eq. (6), may be expressed as

$$d=v_m[(t_2-t_1)+(t_1-t_2+t_3)/(m+1)]. \tag{10}$$

This shows that the effective duration of the trapazoidal stress pulse is

$$\Delta t'=t_2-t_1+(t_1-t_2+t_3)/(m+1). \tag{11}$$

Thus, a corrected dislocation velocity v' may be defined for each value of actual dislocation displacement d at the loaded end by

$$v'=\frac{d}{\Delta t'}=d\left[t_2-t_1+\frac{(t_1-t_2+t_3)}{(m+1)}\right]^{-1}, \tag{12}$$

where the "best fit" value of m is to be employed. Values of corrected dislocation velocity for each test, computed by means of Eq. (12) using $m=0.7$ are given in the fourth column of Table II.

The values of corrected dislocation velocity, v', are plotted as a function of the experimentally determined maximum resolved shear stress during the stress pulse τ_m in Fig. 7. The solid line in Fig. 7 represents the "best fit" velocity versus stress relation given by Eq. (8). The vertical lines through the plotted points represent the uncertainty in dislocation displacement d associated with the extrapolation procedure used to obtain d from the measurements in Fig. 6.

The sensitivity of the "fit" between the experimental data and the choice of the velocity exponent m may be shown by arbitrarily assuming the attractive value $m=1$. Then the other material constant τ_0 may be chosen so as to minimize the mean displacement error as given by Eq. (7). When this is done it is found that $\tau_0=2.7\times10^4$ dyn/cm^2, and the mean displacement error is $e=0.209$. Furthermore, new values of the corrected

dislocation velocity v' may be computed using the value $m=1$ in Eq. (12). These values of corrected dislocation velocity corresponding to a velocity exponent of $m=1$ are given in the fifth column of Table II and plotted versus maximum resolved shear stress in Fig. 8. The corresponding dislocation velocity vs stress relation,

$$v=v_0(\tau/2.7\times10^4)\ \text{cm/sec}, \qquad (13)$$

is shown by the solid line in Fig. 8.

DISCUSSION

The foregoing results show that when the data obtained in these experiments are fit to a power-law functional relationship between dislocation velocity and resolved shear stress, Eq. (5), the "best fit" is obtained by employing a stress exponent, $m=0.7$. The "fit" is not quite as good if it is assumed that the exponent is $m=1$. However, the scatter and uncertainty in the experimental measurements are such that the value $m=1$ may be the true value. Thus, the resistance to the motion of individual dislocations in 99.999% pure copper may be described approximately as a simple linear viscosity, at least in the dislocation velocity range of 100 to 1000 cm/sec.

Various investigators have suggested forms other than Eq. (5) for the dislocation velocity vs stress relationship. The theory of Gilman[13] involving point-defect drag and, consequently short-range interactions, is an attractive description for dislocation mobility in copper. This theory predicts a dislocation velocity vs stress relationship of the form

$$v=c_s\exp(-\text{constant}/\tau), \qquad (14)$$

where c_s is the velocity of propagation of elastic shear waves in the material. However, the limiting velocity, found by extrapolating a plot of the values of $\ln v$ vs $1/\tau_m$ obtained from this investigation, is $c_s=10^3$ cm/sec rather than the actual shear wave velocity of 2.14×10^5 cm/sec.

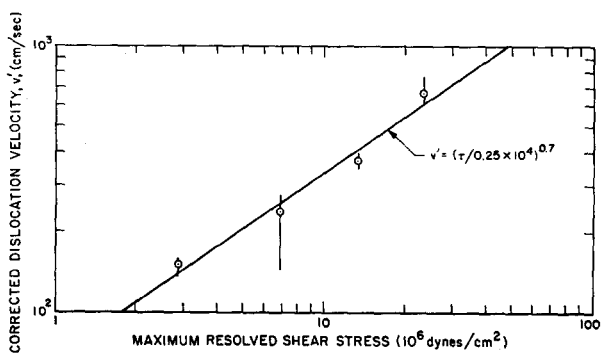

FIG. 7. Corrected dislocation velocity vs maximum resolved shear stress, for $m=0.7$.

[13] J. J. Gilman, J. Appl. Phys. **36**, 3195 (1965).

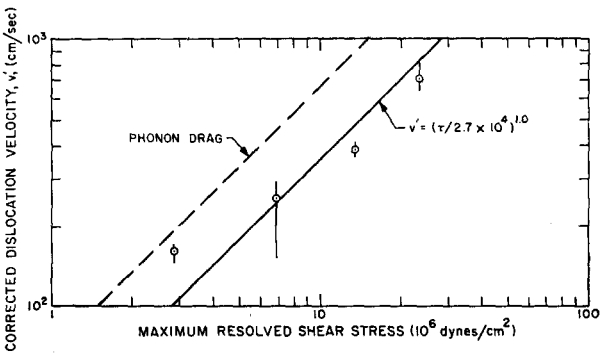

FIG. 8. Corrected dislocation velocity vs maximum resolved shear stress, for $m=1.0$.

The theory of Fleischer[14] is based upon the idea that dislocation velocity is governed by the interaction between dislocations and point defects which produce large tetragonal lattice distortions such as result from the introduction of carbon into iron. The mobility data for copper does not extend over a sufficiently large range of velocity and stress to permit a good test of the functional dependence predicted by Fleischer's theory. The relative insensitivity of the flow stress of copper to temperature would appear to rule out this theory however.

Another mechanism which can limit the velocity of dislocations is the interaction between the moving strain field and the thermal vibrations of the crystal lattice, commonly known as the phonon drag or phonon-viscosity effect. Leibfried[15] was the first to estimate the drag on a screw dislocation moving at a constant velocity caused by the scattering of phonons. Lothe[16] reviewed and extended this estimate and concluded that for metals Leibfried's result is correct and should be about the same for edge- and screw-oriented dislocations. Lothe estimates that the effects of anharmonicity in the core region, the phonon viscosity (lattice vibrations considered as a viscous phonon gas), and the scattering of phonons are each of the same magnitude. The total of these three effects gives a drag stress τ_d at ordinary temperatures, $T>\theta$ (where θ is the Debye temperature) of

$$\tau_d\approx(3\epsilon/10)v/c_s, \qquad (15)$$

where ϵ is the thermal energy density, c_s is the shear wave velocity, and v is the dislocation velocity. Thus the phonon interaction theory predicts a linear stress dependence of dislocation velocity, in reasonable agreement with our experimental results.

The thermal energy density, ϵ in Eq. (15), is assumed to be given by the relation

$$\epsilon=3kT/(a^3/z), \qquad (16)$$

[14] R. L. Fleischer, J. Appl. Phys. **33**, 3504 (1962).
[15] G. Leibfried, Z. Physik. **127**, 344 (1950).
[16] J. Lothe, J. Appl. Phys. **33**, 2116 (1962).

TABLE III. Dislocation damping constant in copper at room temperature (10^{-4} dyn·sec/cm^2).

This study	7
Alers and Thompson[19]	8
Stern and Granato[18]	6.5
Suzuki *et al.*[20]	0.79

where a = the lattice parameter = 3.6×10^{-8} cm, and z = the number of atoms per unit cubic-lattice cell = 4. The drag stress calculated from Eq. (16) is about 55% of the measured values as shown by the dashed curve in Fig. 8. Mason[17] has also treated the effect of phonon viscosity on dislocation motion, and his theory predicts the same order of magnitude of the drag stress as does the theory of Leibfried, but gives a somewhat modified temperature dependence.

Those theories which depend upon thermally assisted dislocation motion, such as Fleischer's,[14] predict that dislocation velocity decreases with decreasing temperature, whereas those theories that depend upon the existence of a drag stress due to phonon scattering and viscosity predict that the dislocation velocity will increase with decreasing temperature. Stress pulse tests on copper specimens at low temperatures, which are in progress, should enable one better to select between the two type of theories of dislocation mobility.

An indirect method of obtaining the drag force on a moving dislocation is based on measurements of internal friction. The theory of Granato and Lucke, briefly reviewed in Ref. 18, has been used to obtain the damping constant B, which is defined as the drag force per unit length of dislocation per unit velocity. The damping constant, given by $B=b\tau_0/v_0$ in the notation used here, is $B=7\times10^{-4}$ dyn·sec·cm^{-2}, when the value $\tau_0=2.7\times10^4$ dyn/cm^2 from Eq. (13) and the known Burgers vector, $b=2.55\times10^{-8}$ cm are employed. Alers and Thompson,[19] Stern and Granato,[18] and Suzuki *et al.*[20] have reported values of B at room temperature based on internal friction measurements and an estimate of the dislocation density of their specimens. These values are listed in Table III together with the directly determined value from this investigation. Thus the dislocation damping constant derived from the results of this investigation is in good agreement with most of the values determined from internal friction measurements. This agreement is especially interesting in view of the fact that the dislocation displacements in this investigation are several orders of magnitude greater than those in the internal friction experiments.

The mobility of dislocations at the yield stress in copper is markedly different from that in other materials for which direct data exists. Table IV lists the yield stress, dislocation velocity at the yield stress, and mobility exponent of a number of materials. The relatively high velocity of dislocations in copper, combined with a low mobility exponent, m, is evident. The small rate sensitivity of the flow stress in copper must therefore be due to a strong stress dependence of the density of moving dislocations in copper. Adams[21] suggested that a strong stress dependence of the moving dislocation density comes about when the internal stress amplitude is comparable in magnitude to the applied stress. When the internal stress amplitude is comparable in magnitude to the applied stress, dislocations will be trapped whenever the total stress drops to zero, and very small changes in the applied stress can change the velocity of a significant number of dislocations from zero to the relatively high value corresponding to the applied stress. The rate sensitivity of the flow stress is thereby very small.

The theory of yielding of a single crystal proposed by Johnston[22] states that for a small mobility exponent and a low density of moving dislocations, there will be a large yield drop when a stress–strain test is performed on the material. The density of mobile dislocations was assumed to be a function of strain but not explicitly a function of stress. Except in special cases, there is no yield drop in a stress–strain test of a copper crystal. Therefore, there must be a large density of moving dislocations at the flow stress, i.e., there must be weak pinning of aged dislocations compared to that provided by interstitials in bcc metals and divalent ions in lithium fluoride and sodium chloride.

SUMMARY AND CONCLUSION

Dislocations in copper move at high velocities at low stresses, and the velocity–stress relation is approximately linear. The low strain-rate sensitivity of the flow stress is attributed to a strong stress dependence of the density of moving dislocations and to the high

TABLE IV. Dislocation velocity at the yield stress (at room temperature unless otherwise noted).

Material	Yield stress (10^6 dyn/cm^2)	Velocity at yield stress (cm/sec)	Mobility exponent m
Tungsten[5]	730	0.001	4.8
Lithium fluoride[1]	88	0.015 (edge) 0.0009 (screw)	25
Sodium chloride[4]	17	0.00001	8
(high purity)	2.9		17
Iron–3% silicon[2]	1200	0.0000015	35
Germanium (500°C)[6]	280	0.0006	1.9
Copper	5	200	0.7

[17] W. P. Mason, J. Acoust. Soc. Am. **32**, 458 (1960).
[18] R. M. Stern and A. V. Granato, Acta Met. **10**, 358 (1962).
[19] G. A. Alers and D. O. Thompson, J. Appl. Phys. **32**, 283 (1961).
[20] T. Suzuki, A. Ikushima, and M. Aoki, Acta Met. **12**, 1231 (1964).
[21] K. H. Adams, Ph.D. thesis, California Institute of Technology, Pasadena, California, 1965 (unpublished).
[22] W. G. Johnston, J. Appl. Phys. **33**, 2716 (1962).

velocities at low stresses, rather than to a large mobility exponent.

The present theories of dislocation mobility may be divided into two categories: one which assumes that dislocation motion is thermally assisted; the other, that thermal assistance is negligible and that interaction with lattice vibrations causes a major portion of the drag force on a moving dislocation. The form of the velocity–stress relationship observed in copper is in qualitative agreement with the latter theory. Further, this theory predicts drag stresses of about 55% of the measured values. This is considered to be good quantitative agreement between theory and experiment in view of the probable accuracies of both theory and experiment.

A more definitive differentiation between the thermally activated and the phonon viscosity mechanisms of dislocation mobility in copper may be obtained from measurements of the temperature dependence of dislocation velocity which are now in progress.

JOURNAL OF APPLIED PHYSICS VOLUME 38, NUMBER 9 AUGUST 1967

Effect of Particle Size on the Colloid Band in CsBr†

RICHARD E. JENSEN
Arizona State University, Tempe, Arizona

(Received 18 January 1967; in final form 27 March 1967)

The effect of particle size on the half-width of the colloid band in CsBr is discussed. Boundary scattering of electrons predominated for small particles and radiation damping for large particles, yielding broad half-widths. For intermediate-sized particles, bulk relaxation effects predominated and the half-width was a minimum. Variations in the minimum half-width in different specimens and the lack of the expected temperature dependence indicated the presence of impurities in the colloidal particles. Electron-microscope observations revealed that the particles were spherical. The colloid band occurred at 1050 nm as compared with the predicted position at 960 nm. Comparison of the observed colloid-band positions in the alkali halides with the predicted positions reveals a systematic difference, the reason for which is not known.

An investigation into the effect of particle size on the colloid band in CsBr is described. The first section discusses the effect of particle size, through boundary scattering and radiation damping, on the half-width and temperature dependence of the colloid band. A brief description of the experimental methods is given, followed by the results which are compared with the theory.

I. THEORY

The theoretical plasma frequency for ellipsoidal metal particles, much smaller than a wavelength of light and the skin depth, has been given by Doyle[1] and in mks units is

$$\omega_0^2 = (nq^2L/m\epsilon_2)\,(1-L+L\kappa_e/\kappa_2)^{-1}. \qquad (1)$$

This result assumes the Drude theory for metals, where n = electron concentration, q = electron charge, m = electron mass, ϵ_2 = permittivity of the medium surrounding the particles, κ_2 = dielectric constant of the medium, κ_e = dielectric constant due to the metal ion cores, and L = the depolarization constant which depends on the particle shape. For spheres, $L=\frac{1}{3}$ and the Mie theory[2] is valid. For very small spherical particles the Mie theory is identical to that discussed by Doyle and it is only when the particle size approaches the skin depth that significant differences occur.

The half-width of the extinction band is equal to $1/\tau$, where τ is the relaxation time for electrons in the particles. The relaxation time depends on the particle size and is given by

$$\tau^{-1} = (u/\Lambda) + \tau_B^{-1} + [\omega_0 V/6\pi L(\lambda_2)^3], \qquad (2)$$

where u = velocity of an electron at the fermi surface, Λ = mean free path in the bulk metal, $1/\tau_B$ = damping term due to boundary collisions, V = volume of the particle and λ_2 = (plasma wavelength in the medium)$/2\pi$. The first term corresponds to normal electron relaxation in the bulk metal, the second term to electron collisions with the boundary, and the third term to radiation damping was given by Gossick.[3] According to Doyle,[4] the damping term due to boundary collisions for spherical particles is

$$1/\tau_B = u/a, \qquad (3)$$

where a = radius of the particle. Figure 1 shows the theoretical variation of the half-width of the colloid band for Cs particles in CsBr with particle radius,

† This work was completed while the author held a National Science Foundation Cooperative Graduate Fellowship.

[1] W. T. Doyle, Proc. Phys. Soc. (London) **75**, 649 (1960).

[2] G. Mie, Ann. Phys. **25**, 377, (1908). W. T. Doyle and A. Agarwal [J. Opt. Soc. Am. **55**, 305 (1965)] discuss this theory as applied to small particles,

[3] B. R. Grossick, *Proceedings of the Interdisciplinary Conference on Electromagnetic Scattering, Potsdam, New York 1963* (Pergamon Press, Inc., NewYork, 1963), p. 417.

[4] W. T. Doyle, Phys. Rev. **111**, 1067 (1958).